Applied Surface Science 600 (2022) 154087

Contents lists available at ScienceDirect

Applied Surface Science

journal homepage: www.elsevier.com/locate/apsusc

Full Length Article

Copper adatoms mediated adsorption of benzotriazole on a gold substrate

Federico Grillo [a,*], Chiara Gattinoni [b], Christian R. Larrea [a], Paolo Lacovig [c], Neville V. Richardson [a]

[a] EaStCHEM-School of Chemistry, University of St. Andrews, St. Andrews KY16 9ST, United Kingdom
[b] Department of Chemical and Energy Engineering, London South Bank University, London SE1 0AA, United Kingdom
[c] Elettra – Sinctrotrone Trieste, S.C.p.A., S.S. 14 km 163.5, 34149 Basovizza, Trieste, Italy

ARTICLE INFO

Keywords:
Corrosion inhibitors
Copper adatoms
Gold
Benzotriazole
HREELS
XPS
NEXAFS
STM
DFT

ABSTRACT

The adsorption of organic molecules on metal surfaces is often mediated by metal adatoms, however their effect on the geometry of the resulting supramolecular structure can be difficult to determine. Herein, the role played by reactive copper atoms in the adsorption chemistry of benzotriazole (BTAH), an organic corrosion inhibitor for copper well-known for forming adatom mediated supramolecular structures, on an inert substrate, Au(1 1 1), has been investigated in an ultra-high vacuum environment using a combination of complementary surface sensitive techniques and density functional theory calculations. Pseudo-ordered and hydrogen bonded flat-lying assemblies convert into ordered -[CuBTA]$_n$- flat-lying organometallic species of well-defined stoichiometry upon addition of copper atoms from the gas phase onto an Au(1 1 1) surface, which has been pre-dosed with BTAH. The formation and characterisation of these organometallic species are discussed in the light of the experimental results and computational modelling. The combination of complementary experimental and computational methods is crucial in order to obtain a thorough characterisation of such a complex system. The final supramolecular structure shows previously unseen BTA phases, which are favoured by the adsorption distribution of copper adatoms on Au(1 1 1), and are stable up to 500 K.

1. Introduction

The bottom-up synthesis of extended organic monolayers on metal surfaces has gained considerable research interest because of the possibility of tailoring surface morphologies and functionalities. When organic molecules are deposited on a surface, self-assembly can be regarded as the result of a balance between the different interactions in the system, such as molecule–surface and molecule–molecule interactions, leading to adsorption and rearrangement. The binding of a molecule to a surface may be mediated by the presence of adatoms [1–22], as is the case also for benzotriazole (BTAH, Scheme 1**a**), a well-known corrosion inhibitor for copper and its alloys [23–40].

Often the presence of adatoms is inferred from the spacing between STM features, without a direct observation [7,9–22]. Single adatoms can seldom be identified when isolated [18–20], in an organometallic compound [17,19,21], or when they form small clusters [12]. In contrast, the role of hetero-adatoms, that is adatoms that are chemically different from the metal substrate [9–22], can be assessed directly, for example via XPS, and their surface concentration can be easily varied [14]. Moreover, chemically equivalent but morphologically different structures have been seen to form when hetero-adatoms are dosed after the deposition of the organic species rather than before [18,19]. Thus, it is of great interest to study hetero-adatoms in supramolecular structures, both to clarify the role of adatoms in structures where this is not otherwise clear, as well as to understand the kinetic effects regulating the behaviour of adatoms in adsorbed organometallic complexes.

In this contribution, attention is focused on the effects played by copper atoms, dosed from the gas phase, in the formation of BTAH organometallic assemblies, on Au(1 1 1) surfaces pre-covered by BTAH. A better understanding of the behaviour of BTAH/Cu organometallic complexes has important technological implications. Indeed, understanding the nature of the interactions between BTAH and copper adatoms can lead to the recognition of the fundamental building blocks which form the passivating layer protecting the copper surface from further oxidation, which would ultimately lead to corrosion. In addition to this, rationalisation of the adsorption mechanism can also help in the search for novel corrosion inhibitors based on similar scaffolding, or on similar principles as BTAH, such as, for example, functionalized BTAH

* Corresponding author.
E-mail address: federico.grillo@st-andrews.ac.uk (F. Grillo).

https://doi.org/10.1016/j.apsusc.2022.154087
Received 18 February 2022; Received in revised form 6 June 2022; Accepted 25 June 2022
Available online 27 June 2022

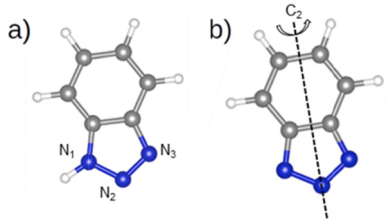

Scheme 1. Chemical structure of (a) benzotriazole (BTAH) and (b) deprotonated benzotriazole (BTA^-); in (a) N atoms are labelled for reference; in (b) the C_2 axis of BTA^- is shown; colour scheme: H, white; C, grey; N, blue.

[39,40] or *N*-heterocyclic carbenes [21–22,41–42].

To unravel the complexity of such a system, a synergistic experimental and computational approach has been employed. Measurements were conducted in an ultra-high vacuum environment, through complementary surface sensitive techniques including scanning tunnelling microscopy (STM), to obtain topographic images of the organometallic structures with molecular resolution, and high-resolution electron energy loss spectroscopy (HREELS), giving information on molecular coordination and orientation. Synchrotron based techniques, such as X-ray photoelectron spectroscopy (XPS) and near edge X-ray absorption fine structure (NEXAFS) spectroscopy were crucial in providing information on the chemical state and orientation of the system. The observed structures are compared with density functional theory (DFT) calculated models and critically discussed in the light of previously proposed adsorption models.

2. Materials and methods

Before exposure to benzotriazole and copper the Au(1 1 1) single crystal was prepared by argon ion sputtering and annealing cycles until a featureless background was seen in HREELS, XPS and large terrace with the characteristic ($22 \times \sqrt{3}$) reconstruction were observed on STM.

BTAH dosing was carried out by simply opening a gate valve separating a quartz crucible containing the compound from the main chambers containing the Au(1 1 1) crystal held at room temperature. BTAH has a vapour pressure high enough at room temperature to sublime under UHV conditions [27–28]. Copper was dosed on the Au(1 1 1) surface by electrically heating a high purity copper wire (5 N purity, 0.1 mm diameter) wrapped around a tantalum filament (5 N, 0.25 mm), yielding a deposition rate of ca. 0.07 ML (monolayer) min^{-1} [20,31,43–45]. 1 ML is defined as one copper atom per surface unit cell of Au(1 1 1). The copper coverage was calibrated by following the attenuation of the Au $4f_{7/2}$ surface component on XP spectra.

HREEL measurements (VSW HIB 1001 double-pass spectrometer) were carried out in a UHV system with a base pressure better than 1×10^{-10} mbar, in the specular direction ($\theta_i = \theta_s = 45°$, where θ_i and θ_s are the angles formed by the incident, $_i$, and scattered, $_s$, electron beams with the surface normal), with a primary beam energy of 4 eV and a typical elastic peak resolution of ca. 50 cm^{-1} (6.2 meV fwhm).

NEXAFS and XPS measurements were performed at the SuperESCA beamline [46–47] of the Elettra third generation synchrotron radiation source in Trieste, Italy. The experimental chamber was equipped with a Phoibos hemispherical energy analyzer (SPECS GmbH) with a home-made delay-line detector [48] and has a background pressure of about 2×10^{-10} mbar. NEXAFS data were collected by monitoring the yield of N KLL Auger electrons at 380 eV. Data were recorded for angles of incidence in the range $20° \leq \theta \leq 90°$; the angle between the photon beam and the electron energy analyser was 70° and the linear polarisation of ca. 100%. Data were normalised following an established procedure that includes dividing the spectrum of the adsorbate covered surface by that of the clean surface [49], having first divided each spectrum by the measured incident photon flux as recorded from a clean gold mesh located close to the main experimental chamber. Post processing, normalization to a step height of 1 unit, and peak fitting were done with the Athena package [50]. Angular dependency and estimation of the orientation of the molecular plane were addressed according to refs. [49] and [51].

Core level XP spectra were recorded with the sample at room temperature, and at photon energies of 320 eV (Au 4f), 400 eV (C 1s), 500 eV (N 1s), or 1050 eV (Cu $2p_{3/2}$) with an overall energy resolution better than 100–250 meV. At these photon energies, the kinetic energy measured by the analyzer is around 100 eV, allowing one to assume an approx. constant transmission function for the analyzer. Binding energies were referenced to the Fermi level recorded for each photon energy. XP spectra were used to verify surface cleanliness. Possible X-ray induced overlayer damage was minimized by probing the sample at different surface locations for each measurement. Data fitting was done using the CasaXPS software [52]. For the peak fitting a Shirly-type background was subtracted and Gaussian-Lorentzian shapes were used (typically Gaussian with a 35% of Lorentzian). In the quantitative determination of the stoichiometric ratios, the raw intensities were normalised by the respective photon flux and the following normalised cross-sections were used: C 1s 1, N 1s 0.925, Cu 2p 1.210 [53–54]. The data shown here are those calculated in the dipole length approximation.

STM (VT-STM Omicron) experiments were performed in UHV with base pressure better than 1×10^{-10} mbar; scanning was done in constant current mode, at room temperature, using home-made electrochemically etched tungsten tips. Images were processed using the WSxM software package [55].

Simulations of copper adsorbed on BTAH pre-covered Au(1 1 1) have been optimized using VASP [56,57] with the optB86b-vdW functional [58] and the projector augmented wave (PAW) method [59]. The kinetic energy cutoff on the basis set was 400 eV. Periodic images were separated by ca. 20 Å vacuum and the atomic coordinates of the bottom two gold layers were kept fixed at bulk values. Convergence of all the settings was thoroughly checked. The Monkhorst-Pack k-point mesh for *fcc* Au bulk is $12 \times 12 \times 12$, giving a lattice constant $a_{DFT} = 4.17$ Å, in good agreement with the experimental one $a_{exp} = 4.07$ Å.

Four-layer-thick Au(1 1 1) slabs were used. High coverage structures along the $[1\bar{1}0]$ direction have a surface area of 3×2 unit cells (uc), while along the $[11\bar{2}]$ direction structures with 5×2 uc, 6×2 uc, 7×2 uc and 3×2 uc surface areas were tested. Isolated dimers were also tested in unit cells of 7×7 uc surface area. It was observed that the preferred position of copper adatoms on the Au(1 1 1) surface is in the three-fold hollow site, in good agreement with previous literature [60]. Adsorption on bridge and on top sites were found energetically more costly, by 0.03 eV and 0.8 eV respectively.

The free energy of adsorption has been used to evaluate the energetic stability of the two consecutive adsorption processes which are examined in this work, formation of BTAH hydrogen-bonded chains first, which convert into organometallic chains upon addition of copper atoms from the gas phase and release of hydrogen, are described with the two following reactions:

$$nBTAH + Au(111) \rightarrow \text{-}[BTAH]_n\text{-}/Au(111) \quad (1)$$

$$\text{-}[BTAH]_n\text{-}/Au(111) + mCu \rightarrow \text{-}[CuBTA]_{m,n}\text{-}/Au(111) + \frac{n}{2}H_2 \quad (2)$$

where $\text{-}[BTAH]_n\text{-}$ and $\text{-}[CuBTA]_{m,n}\text{-}$ indicate the hydrogen bonded and organometallic polymer respectively, n is the number of BTAH molecules and m is the number of gas phase copper atoms; when $n \approx m$ (derived from XPS, see section 3.1.2), hydrogen bonded BTAH chains and copper atoms are quantitatively converted into organometallic chains. In the present modelling work, $m = n = 2$. A more complete description of this simplified scenario is reported in SI1.

The free energies for reaction (1) and (2), E_1 and E_2, can be approximated as [61,62] (full derivation in SI1):

$$E_1 = \frac{1}{A_1}\left(E_{\text{-}[BTAH]_n\text{-}/Au(111)} - nE_{BTAH} - E^1_{Au(111)}\right) \quad (3)$$

$$E_2 = \frac{1}{A_2}\left(E_{\text{-}[CuBTA]_{m,n}\text{-}/Au(111)} + \frac{n}{2}E_{H_2} - mE_{Cu} - A_1E_1 - nE_{BTAH} - E^2_{Au(111)}\right) \quad (4)$$

where A_1 and A_2 are the surface areas of the unit cell for the -$[BTAH]_n$-/$Au(111)$ and -$[CuBTA]_{m,n}$-/$Au(111)$ systems, respectively (shown in SI1). The total energies are $E_{\text{-}[BTAH]_n\text{-}/Au(111)}$ for the hydrogen bonded chains, $E_{\text{-}[CuBTA]_{m,n}\text{-}/Au(111)}$ for the system of organometallic chains, E_{BTAH} for the BTAH molecule in the gas phase, $E^1_{Au(111)}$ and $E^2_{Au(111)}$ for the Au(1 1 1) slabs of surface area A_1 and A_2, E_{H_2} for a gas phase dihydrogen molecule and E_{Cu} for a single copper atom in the gas phase. Equation (3) corresponds to the free energy of adsorption of hydrogen bonded BTAH molecules on Au(1 1 1), Equation (4) to the energy change when the hydrogen bonded chains transform into organometallic chains upon deposition of gas phase copper atoms and release of hydrogen to the gas phase. Negative free energies of adsorption indicate increased stability.

Adsorption energies, E_{ads}, of BTA species are calculated as:

$$E_{ads} = \left(E_{\text{-}[CuBTA]_{m,n}\text{-}/Au(111)} - nE_{BTA} - E_{Cu_m/Au(111)}\right)/n \quad (5)$$

where E_{BTA} and $E_{Cu_m/Au(111)}$ are, respectively, the total energies of the BTA species in the gas phase and of the fully relaxed Au(1 1 1) substrate with m copper adatoms.

XPS core shifts for N 1s were calculated with VASP in the final state approximation using a modified PAW method [63]. The core electron binding energy, E_B, is calculated as the difference between the total energies of the final (excited) state, E_F, and the initial (ground) state, E_I : $E_B = E_F - E_I$. The specific quantity reported herein is the binding energy shift, ΔE_B, relative to a reference system, $E_{B,ref}$: $\Delta E_B = E_B - E_{B,ref}$. As a reference system the atom closer to the surface was chosen. The model N 1s XP spectra were generated from the shifts by the superposition of Gaussian peaks with full width at half maximum fwhm 0.95 eV. It has been shown that XPS simulations using this method provide an excellent signature of the binding structure of the azole moiety to the substrate [30].

Geometrical optimization and frequency calculation of gas phase species were done with Gaussian 09, [64], using DFT, B3LYP, 6-311g, under the assumption of a weak interaction with the surface, as was also the case for adsorption of BTAH on Au(1 1 1) [65], and Cu/Au(1 1 1) [31].

3. Results and discussion

3.1. Experimental

3.1.1. HREELS

After initially dosing BTAH to saturation onto the Au(1 1 1) surface, as reported in Fig. 1, spectrum a), the vibrational spectrum is dominated by the energy loss signals of flat lying, hydrogen-bonded interlocked species [65]. Table 1 summarises the observed vibrations and their assignments. A comparison with calculated spectra is reported in SI2.

For flat-lying molecules characteristic vibrations are observed at 265 cm^{-1} (shoulder) corresponding to an out-of-plane (oop) buckling mode of the full molecule; at 410 cm^{-1}, 520 cm^{-1} and 560 cm^{-1} due to 6- and 5- member rings out-of-plane deformations; at 750 cm^{-1} assigned to the strong C-H out-of-plane bending mode. A raised background in the 1000 – 1500 cm^{-1} range accounts for weak C-N and C-C in-plane related vibrations. A further signature of the flat orientation of the BTAH molecules is the absence of the vibrational modes related to the N-H group. Indeed, in a parallel adsorption geometry, the N-H stretch (ca. 3500 cm^{-1}) is essentially dipole inactive, as is the in-plane bend at ca. 1560 cm^{-1}. An N-H oop bend expected at ca. 690 cm^{-1} is dipole active, yet very weak, because of hydrogen bonding between the molecules.

Upon addition of ca. 0.2 monolayer equivalent of gas phase copper atoms (Fig. 1, spectrum b), no dramatic changes are seen in the energy loss spectrum; the main difference is the appearance of a peak at 1445 cm^{-1}, and a slightly higher background in the ν CH region at around 3000 cm^{-1}. This indicates that most of the adsorbed species still have their molecular planes almost parallel to the surface, in agreement with both STM and NEXAFS observations and the calculated model, as will be shown later. A different vibrational spectrum has been observed previously when molecular species are coordinated with the copper surface and adsorbed in an upright configuration [26,27,66]. With annealing to 340 K (Fig. 1, spectrum c), a further vibration appears at ca. 1115 cm^{-1}. On the ν CH region, a broad peak at ca. 2890 cm^{-1} and a sharp peak at 3080 cm^{-1} are now more evident. The spectrum seen after annealing to 420 K (Fig. 1, spectrum d) shows a general decrease in total intensity, which is attributed to desorption of weakly bound species. In particular, the vibrations at 410, 505 and 560 cm^{-1} disappear, whereas new signals appear at 380 and 460 cm^{-1}. The CH wagging mode at 750 cm^{-1} shows the more significant attenuation and develops a peak at 675 cm^{-1}, which is attributed to an oop mode of the triazo group. Additional vibrations are seen at ca. 965 cm^{-1}, 1250 cm^{-1}, 1440 and 1585 cm^{-1}. A peak at 3055 cm^{-1} becomes more evident. The spectral changes observed upon annealing render evident a change in coordination of BTAH with respect to copper, as will be shown later; the overall change in γ/ν CH, as well as the difference in the out-of-plane deformations of the benzene ring (410 – 560 cm^{-1}), can be interpreted as a reorientation from a flat-lying to a slightly more tilted geometry.

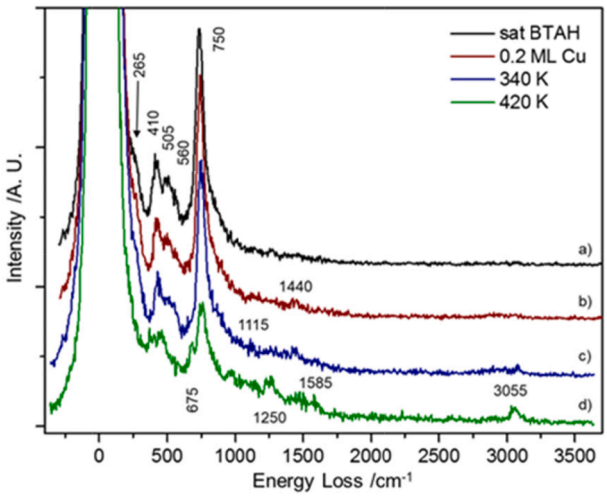

Fig. 1. HREEL spectra following exposure of an Au(1 1 1) surface to BTAH to saturation, addition of ca. 0.2 ML of Cu, and annealing to the indicated temperatures. Spectra are normalised to the intensity of the elastic peak and offset for clarity.

3.1.2. XPS

Fig. 2 shows XP spectra following dosing of the Au(1 1 1) surface with BTAH to saturation, then adding copper to ca. 0.2 ML equivalent and annealing. After preparation (panels b), a Cu $2p_{3/2}$ peak is recorded at 931.9 eV (with a full width at half maximum, fwhm, of 1.2 eV). Since Cu (0) and Cu(I) have similar binding energy (BE) [72–74], it is difficult to determine unambiguously the copper oxidation state a priori, and often the evaluation of the copper oxidation state is made considering the Cu LMM Auger lines [75–79]. However, as very reactive copper atoms are deposited, the symmetric and narrow shape of the observed Cu $2p_{3/2}$ peak and its BE value indicate that copper is more likely to be in the +1 oxidation state. The absence of a peak at higher BE and of a satellite structure at ca. 945 eV [72–75,77–79] (not shown) rule out the presence of Cu(II). As a comparison, upon adsorption of copper on Au(1 1 1), a partial charge transfer from the copper atoms to the gold surface occurs [43–45], but a formal net charge cannot be attributed to copper.

Table 1
Observed energy losses and assignments /cm^{-1}.

mode	sat BTAH	0.2 ML Cu	340 K	420 K	Ref.
ν CH			2980, 3080	2980, 3055	[26,29,31,33,66–68]
ν CC + ν CN + δ CH				1585	[27,31]
ν C_6H_4 ring + δ CH		1440	1440	1440, 1480	[26,27,31,33,69–70]
ν NNN in N—Cu(I)				1250	[27,31,71]
ν NNN + ν CH			1115		[26,31,33,69–70]
δ CH				965	[26,27,31,33,69]
γ CH	750	750	750	740	[27,31,33,66,68]
δ NNN				675	[31,68]
γ C_6H_4 ring	560	560	560		[27,31,68]
γ C_6H_4 ring	505	505	505		[27,31,68]
γ C_6H_4 ring				460	[27,31,68]
γ C_6H_4 ring	410	410	410		[27,31,68]
ν Cu-N_1				380	[27,69]
whole molecule buckling	265	265	265	265	[27,31,68]

ν stretch, γ out-of-plane bend, δ in-plane bend.

However, a more important effect occurs when copper atoms react with BTAH to form organometallic compounds. In fact, upon exposure of Cu/Au(1 1 1) to BTAH, copper oxidises to Cu(I) [31]. The determination of the +1 oxidation state is also in agreement with what was observed on previous studies on adsorption of BTAH on Cu(1 1 1) [30], and Cu(1 1 0) [66] surfaces.

The N 1s region shows a signal which is best fitted with three components having respective maxima at 399.2 eV, 400 eV and 400.8 eV (fwhm 0.7 eV) and an area ratio of 1.9:1.4:1. A Cu:N ratio of ca. 1:6 is calculated, which corresponds to two BTA species per copper atom. Furthermore, the C 1s region shows a signal which is best fitted with three components with maxima at 284.2 eV, 284.9 eV and 285.5 eV (fwhm 0.6 eV) and an area ratio of 4.6:2.8:1. The carbon to nitrogen ratio is calculated as 2.4:1 (expected 2:1). The shapes of both N 1s and C 1s peaks are in agreement with those observed for oversaturated layers of BTAH on Cu(1 1 1) [30], Cu/Au(1 1 1) [31] and Cu(1 1 0) [66]. Such shapes were interpreted as an indication that the molecular layer is formed by a combination of various chemisorbed organometallic $Cu_x(BTA)_y$ species, adsorbed at varying angles with respect to the surface, and flat lying hydrogen bonded species [30,66]. Table S2 shows N 1s and C 1s binding energy values (eV), for BTAH and selected organometallic compounds (see SI3). On annealing (panels c) to 393 K the Cu $2p_{3/2}$ peak position stays almost constant (931.95 eV), while its fwhm decreases slightly (1.12 eV). Both N 1s and C 1s regions lose their respective higher binding energy components. The N 1s region can now be fitted with two components at 399.1 eV and 399.9 eV, fwhm 0.7 eV, with an area ratio of ca. 1.6:1 (expected 2:1). The obtained peak ratio is inverted with respect to that recorded following adsorption on clean Au (1 1 1) [65], but similar to that observed for BTAH/Cu/Au(1 1 1) [31]. A previous study on BTAH pellets had also observed two N components in the XP spectra; the peak component at 399.5 eV was assigned to the N surrounded by other N atoms (N_2 with reference to Scheme 1a), while the component at 400.5 eV was ascribed to N bonded with C ($N_{1/3}$ with reference to Scheme 1a) [79]. In the present case, the observation of a doublet after annealing suggests that the nitrogen atoms in the triazole ring are in different chemical environments also when BTAH reacts with copper. The inverted ratio with respect to adsorption on clean Au(1 1 1) [65] and solid phase BTAH [79], implies that BATH behaves differently in the presence of copper, as expected.

Analogously, after annealing to 393 K, also the C 1s region can be fitted with two components at 284.1 eV and 284.8 eV, fwhm 0.51 eV, with an area ratio of ca. 1.5:1 (expected 2:1). The observed ratio is

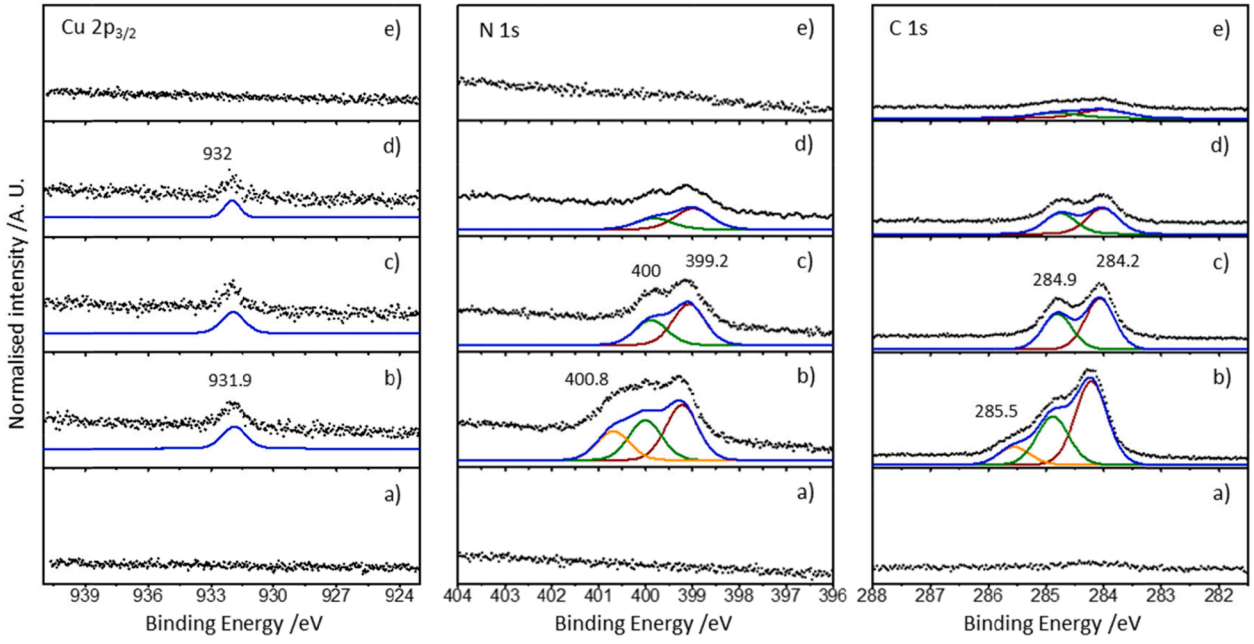

Fig. 2. Cu $2p_{3/2}$, N 1s and C 1s XP spectra before, (a), and following exposure of a Au(1 1 1) surface to BTAH to saturation and addition of ca. 0.2 ML equivalent of Cu, (b), and annealing to 393 K, (c), to 493 K, (d) and to 670 K, (e); data points in black; peak fitting in colours.

similar to that determined upon adsorption on clean Au(1 1 1) [65] and Cu/Au(1 1 1) [31], a clear indication that the benzene ring is in a similar environment. Part of the physisorbed BTAH molecules desorb, leaving on the surface almost exclusively BTA species coordinated with copper. A Cu:N ratio of 1:3.4 is calculated. Considering that each BTA species contains three N atoms, this is interpreted as the presence of an organometallic compound in which the Cu:BTA ratio is ca. 1:1. The C:N ratio remained at 2.4:1, indicating that the BTA(H) species are still intact.

Upon annealing to 493 K (panels d in Fig. 3), an overall decrease in peak intensities is seen, while peak positions, Cu:N and C:N ratios remain almost constant, up to 673 K, when both Cu $2p_{3/2}$ and N 1s signals vanish. Some residual signal is still present in the C 1s region. The changes in intensities and intensities' ratios of the XPS signals with annealing are summarised in Table 2.

The Cu:BTA ratio is in favour of an excess of BTAH; this is expected to manifest as some remaining BTAH diffusing species after addition of copper. However, the presence of some copper clusters is also seen on STM (see 3.1.4). This is ascribed to the difference in the areas sampled by the two techniques, XPS averaging over a much larger area, while the concentrations of the different adsorbed species may vary locally, as revealed by STM. The relative stability of Cu:N and C:N ratios with annealing and the relative decrease of the peaks' intensities can be interpreted as initial desorption of weakly bound BTAH species, followed by some gradual desorption of a $Cu_x(BTA)_y$ compound, with $Cu_x(BTA)_y$ still remaining on the Au(1 1 1) surface. Desorption of an organometallic complex was also observed from Cu(1 1 1) [complete by ca. 600 K, 27], Cu/Au(1 1 1) [stable to 500 K at least, complete by 670 K, 31] and Ni(1 1 1) [complete by ca. 600 K, 80].

3.1.3. NEXAFS

Fig. 3 shows grazing, 55° and normal incidence N K-edge NEXAFS spectra following exposure to BTAH and copper at room temperature (a), and after annealing to 393 K (b) and to 493 K (c), with the 90°-20° difference spectra (d) at each temperature.

With reference to the spectrum collected at an incidence angle of 20° at room temperature (red lines), a detailed π* structure with resonances at 399.4, 399.9, 401.5 and 402.5 eV photon energy and σ* resonances at 406.5 and 411.6 eV photon energies are observed. The room temperature spectra are very similar to those recorded for BTAH deposited on Au (1 1 1) [65] and on Cu/Au(1 1 1) [31], however the fine structure of the π* resonance in the 20° angle spectrum is not as resolved as for Au(1 1 1) and the dichroism is slightly reduced, as a small π* resonance is still present in the normal incidence spectrum, as observed for Cu/Au(1 1 1). The change in the fine structure of the π* resonance is ascribed to the presence of both a hydrogen-bonded and a metal organic compound. A fitting procedure performed on angular dependent measurements (SI4, Figure S4a) gives an average tilt angle of 12° ± 5° for the triazole ring with respect to the surface. This has to be compared with an almost parallel adsorption on Au(1 1 1) [65], and with the adsorption on Cu/Au (1 1 1) where for mixed species adsorbed at various geometries an average angle of 38° ± 5° for the triazole ring was calculated [31]. Upon annealing to 393 K (Fig. 3b), the majority of the flat-lying freely diffusing hydrogen bonded species are desorbed and what remains on the surface are more strongly bound organometallic species. With reference to the spectrum collected at grazing incidence, π* resonances are observed at photon energies of 399.3, 399.9, 401.5 and 402.6 eV, whereas σ* are observed at 406.8 and 411.7 eV. When compared to the adsorption of BTAH on Cu/Au(1 1 1) [31], clear spectral differences are seen. Furthermore, considering the calculations reported in [31], the relative increase of the shoulder at 399.3 eV (*a* in inset Fig. 3d) with respect to that at 399.9 eV (*b* in inset Fig. 3d) in the fine structure π* resonance, is interpreted as the formation of a Cu-N_1 bond. The *a:b* ratio from 0.67 at RT changes to 0.96 after annealing to 393 K. This relative increase is rendered more evident in the inset in the 90°-20° spectra (Fig. 3d). Both the angular dependency and fine structure of the π* region of the NEXAFS features indicate that the organometallic species is adsorbed either at a small angle, calculated as 10° ± 5° (SI4, Figure S4b), or the majority of which is adsorbed flat, and the small contribution to the dichroism is due to the upright species adsorbed at copper clusters at the elbows of the herringbone reconstruction, as evidenced by STM.

Upon further annealing to 493 K (Fig. 3c), only small changes in the spectra are recorded. Qualitatively, the π* resonance structure remains essentially unaltered, whereas a worsening of the signal-to-noise ratio is seen. With reference to the spectrum collected at a 20° incidence angle, the π* resonances have maxima at 399.5, 399.9, 401.4 and 402.4 eV, whereas σ* resonances are observed at 406.6 and 411.6 eV. The *a:b* ratio stays 0.96, indicating that the overall structure of the adsorbed species does not change. The average tilt angle of the triazole ring with respect to the surface is estimated as 10° ± 5° (SI4, Figure S4c). In line with XPS measurements, for which peak shapes and positions are unchanged, only the areas change, this is interpreted as an easier desorption of the flat-lying $Cu(BTA)_2$ species, the majority of which are on the surface, with those at the herringbone elbows still persistent. At each temperature, the residual intensity of the π* resonance recorded at a normal incidence angle can also be attributed to a minority of molecular species adsorbed at step edges and other surface defects.

3.1.4. STM

As already highlighted, after dosing BTAH to Au(1 1 1) to saturation, hydrogen-bonded flat-lying structures are formed [65, see also Figure S9]. Such structures are not observed at room temperature via STM, because of rapid diffusion [31,65]. Even upon addition of copper, to ca. 20% coverage equivalent, molecular diffusion is still prevalent; however, on annealing to 340 K loosely bound hydrogen-bonded species desorb and molecular features can be resolved, as shown by the STM topographs in Fig. 4. Such features are attributed to organometallic species, indicating that copper atoms play a fundamental role in stabilising the ad-layer structure. The brighter and larger features on the terraces in Fig. 4a are attributed to copper atoms which have condensed on the Au(1 1 1) herringbone elbows to form small clusters, whereas the organometallic species can be observed as a fine structure. Clusters cover ca. 5.2% of the area shown (see SI5), have widths in the range 5 – 12 nm, and their positions match that expected for the elbows of the herringbone reconstruction, measured as 6.4 nm (expected value ca. 6.3 nm) as in profile *c* in Figure S6c. The mass balance with respect to the nominal amount of copper dosed, ca. 20%, is essentially satisfied, considering that clusters are layered (see line profile *a* in figure S6c), copper is incorporated in the organic layer to form the organometallic species, and some migration of copper atoms sub-surface cannot be ruled out [18–20,43–45]. Adsorbed features appear as sequences of elongated protrusions (Fig. 4b, annealed to 420 K).

Table 2
Changes in XPS signals with temperature.

temp /K	Cu $2p_{3/2}$ /%	N 1s /%	C 1s /%	C:N	Cu:BTA	Notes
RT	100.00	100.00	100.00	2.4:1	1:2	As prepared
393	90.06	51.69	52.16	2.4:1	1:1.1	ΔCu −9.94%; ΔN −48.31%; ΔC −47.84%
493	50.21	28.25	29.91	2.5:1	1:1.1	ΔCu −39.85%; ΔN −23.44%; ΔC −22.25%
673	–	–	12.71	–	–	Molecular desorption complete

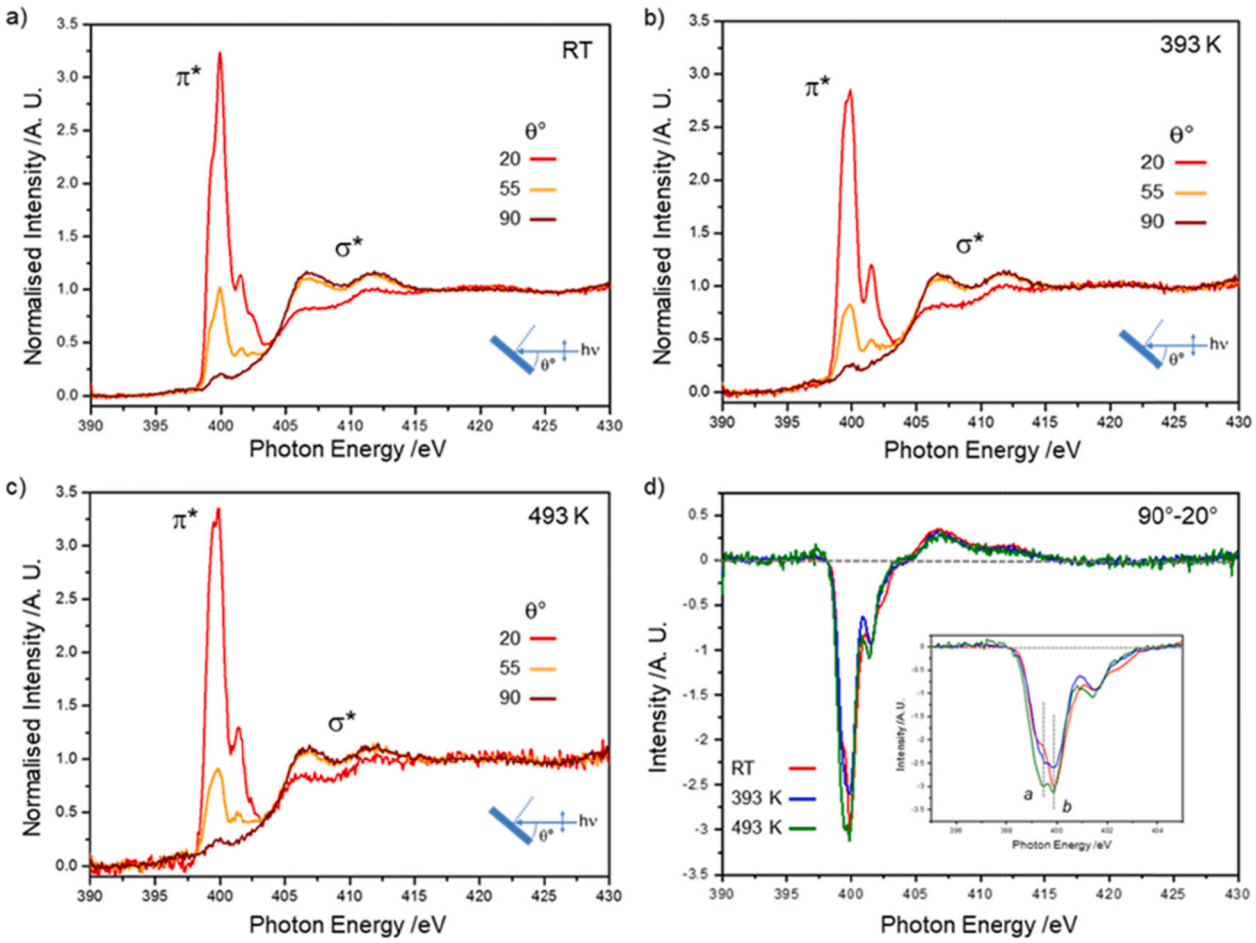

Fig. 3. Angular dependent N-K edge NEXAFS spectra (a) following exposure of an Au(1 1 1) surface to BTAH to saturation and addition of ca. 0.2 ML equivalent of Cu, (b) after annealing to 393 K, (c) 493 K (d), 90°-20° spectra at each temperature. The measurement geometry and the direction of the photon beam polarisation are sketched in the lower right corners of the graphs.

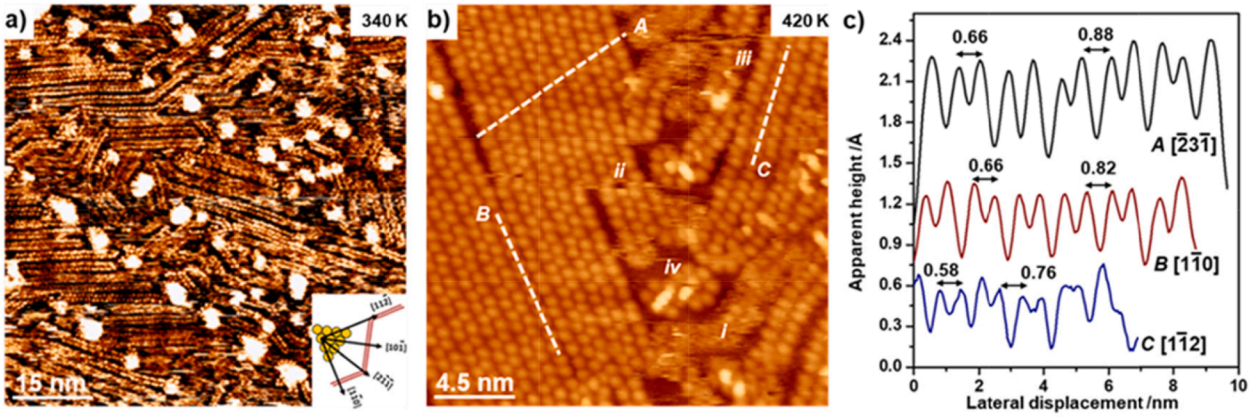

Fig. 4. Topographic STM images showing features produced upon dosing ca. 0.2 ML equivalent Cu on an Au(1 1 1) surface pre-saturated with BTAH; (a) 340 K, 75 × 75 nm^2, −0.8 V, 0.25 nA, surface directions as in the inset; (b) 420 K, *A* along [2̄3̄1], *B* along [1̄10] and *C* along the [1̄12], indicate line profiles reported in (c); *i* indicates diffusing species, *ii* indicates features which have been moved along the fast scanning direction (horizontal), *iii* indicates domain edge features which appear more elongated, *iv* indicates molecular condensation over a copper cluster at the elbow of the herringbone reconstruction, 22.5 × 22.5 nm^2, −1 V, 0.15 nA; (c) *A*, *B* and *C* line profiles as in (b).

Each protrusion is consistent with the molecular dimension of a benzotriazole molecule adsorbing with its molecular plane almost parallel to the surface; an adsorption geometry also indicated by vibrational spectroscopy and NEXAFS measurements. Protrusions appear to pair and form chain-like structures running for several nm and are not confined within the ridges of the herringbone reconstruction, which is almost unperturbed (exception made for some of the elbows which are decorated by the copper clusters) under the ad-layer; its presence has been highlighted in Figure S6. The overview in Fig. 4a) also shows that chains appear to "connect", or to change direction, in correspondence of

herringbone elbows. The majority of the chains on the left side of Fig. 4b follow close packed directions, whereas those on the right end side follow ⟨11$\bar{2}$⟩-type directions. The longer molecular axes appear to be rotated by 60/120° with respect to the direction of propagation of the chain, thus aligned to the same type of directions. The observation of organometallic chains running along the two principal and equivalent crystallographic directions, without a clear preference, points to the energy of adsorption of the chains being similar. Cross section measurements in Fig. 4b, reported in Fig. 4c, help in determining the possible coordination of the adsorbed features. Profile *A*, along the [$\bar{2}3\bar{1}$] direction, runs across 12 rows of molecular features and shows two average spacings of 0.66 nm between maxima next to a shallow valley and 0.88 nm between to maxima next to a deep valley. Profile *B*, along close a packed direction, covers a row of 12 molecules and shows two peak-to-peak distances: 0.66 nm between to maxima next to a shallow valley, and 0.82 nm between maxima next to a deep valley. Profile *C*, along [1$\bar{1}$2], shows average spacings of 0.58 and 0.76 nm. The alternate spacing of the line profiles across the chains may indicate a different mode of interaction every two BTA species, as will be clarified in the modelling section. Copper adatoms do not show STM contrast at the employed scanning condition. Some indication of diffusing species still present on the surface is given by portions of the images showing poor losing resolution of adsorbed features, as indicated in Fig. 4b, *i*. As indicated in Fig. 4b, *ii*, adsorbed features appear to have shifted by about one molecular unit along the fast scan direction (horizontal in figure). Features at the edges of the densely packed areas appear more elongated (Fig. 4b, *iii*), reminiscent of hydrogen bonded BTAH molecules on Au (1 1 1) [65]; such molecules are less constrained by molecular packing and have higher ability to diffuse outward. Brighter features in Fig. 4b, *iv* are ascribed to upright molecules, surrounded by molecules orientated with their molecular planes more parallel to the surface, all condensed over a copper cluster. These recall the features seen at the elbows of the herringbone reconstructions on the BTAH/Cu/Au(1 1 1) system [31]. This small portion of features orientated at a larger angle to the surface is likely contributing to the observation of additional active modes in vibrational spectroscopy and to the determination of the averaged

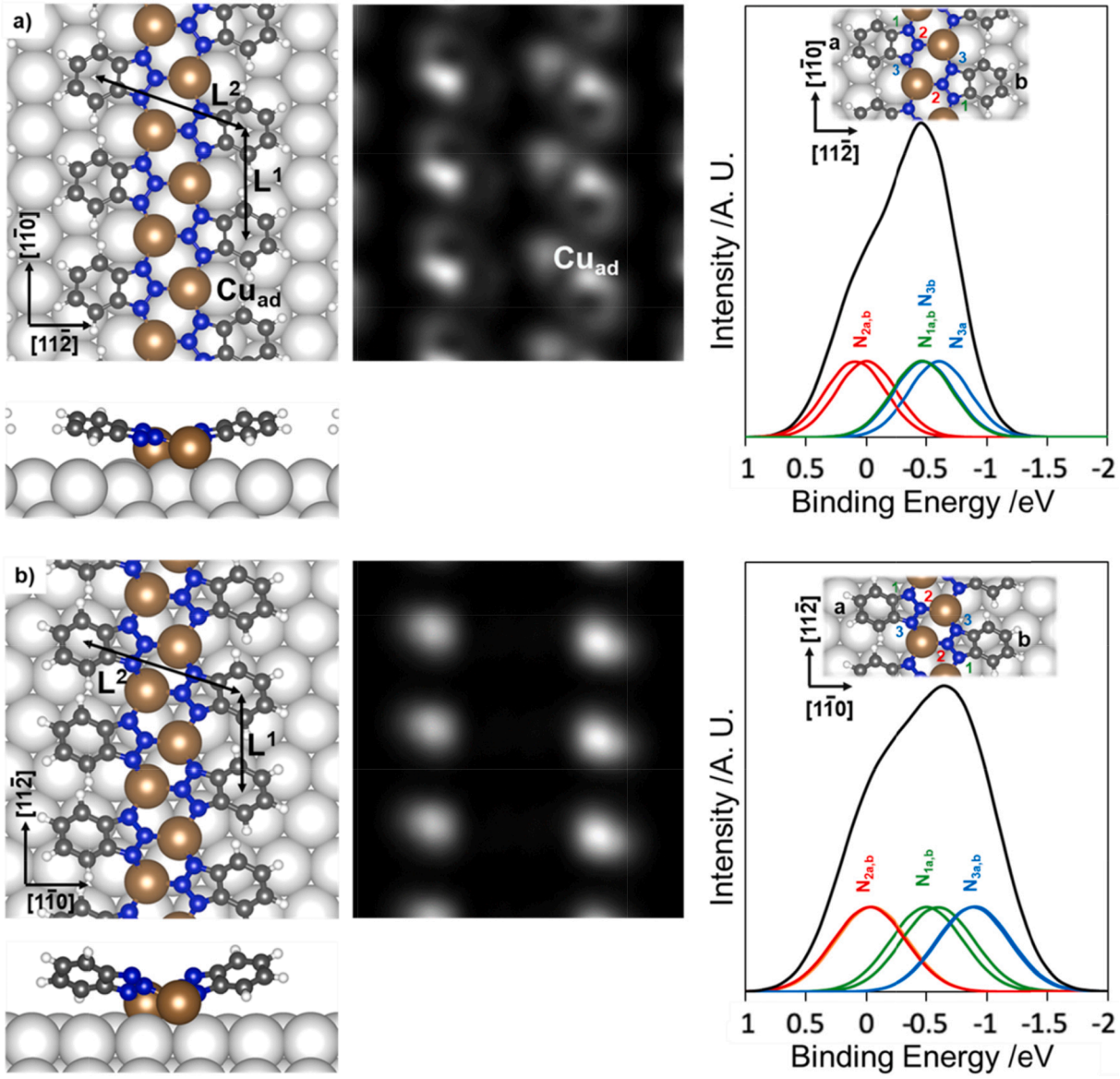

Fig. 5. From left to right: atomistic representation, simulated STM and simulated N 1s XP spectra for two Cu/BTA/Au(1 1 1) systems. (a) Most stable organometallic chain along the [1$\bar{1}$0] direction (and most stable structure overall), (b) most stable organometallic chain along the [11$\bar{2}$] direction. In the right panels, N atoms are labelled as follows: $N_{ia,b}$, where $_i$ indicates the position on the triazole moiety, $_a$ the molecule on the left and $_b$ the molecule on the right. Colour scheme: H, white; C, dark grey; N, blue; Cu adatoms, brown; Au surface, light grey.

dichroism in NEXAFS.

Additional STM images, showing less frequent features and including direct comparison with related systems, are reported in SI5.

3.2. Modelling

Density functional theory simulations were used to investigate the geometry and adsorption energy of benzotriazole adsorbed on Au(1 1 1), before and after the deposition of Cu atoms.

For the Cu/BTA/Au(1 1 1) organometallic complexes a range of structures and coverages were considered, as shown in SI6. Two orientations for the complexes were tested, running along the $[1\bar{1}0]$ and the $[11\bar{2}]$ directions. In contrast with the behaviour of benzotriazole on Cu (1 1 1) [37], structures consisting of two BTA species connected by one copper adatom were not found to be energetically favourable on Au (1 1 1). The most favourable complexes that were observed are organometallic polymeric structures, with a Cu:BTA 1:1 ratio, in agreement with the XPS data collected after annealing (see Table 2), which may bear similarities with the necklace polymer of Ref. [38]. The most stable organometallic chain oriented along the $[1\bar{1}0]$ direction is shown in Fig. 5**a**. All three nitrogen atoms in the azole moiety form a bond with a copper adatom. Copper adatoms, when not bonded to BTA species, reside in a hollow site of the Au(1 1 1) surface (see Materials and Methods), however, when part of the organometallic chains, are pulled out from this site by 0.2 Å in the direction normal to the surface. The benzene-like rings adsorb onto the gold surface via van der Waals interactions keeping the BTA species almost flat on the surface, the tilting angles being around 6-8°, in good agreement with the estimations extracted from the NEXAFS data.

The distance between neighbouring BTA species (the position of a BTA species is taken as the centre of the benzene-like ring) along the $[1\bar{1}0]$ direction (L^1 in Fig. 5a) is 5.9 Å, while between BTA species across the chains (L^2 in Fig. 5a) is 8.7 Å, values which are reasonably close to the measured molecular distances in Fig. 4c, line profile *B*, albeit slightly shorter. Along the $[11\bar{2}]$ direction BTA species form very similar chains (Fig. 5b), the azole N atoms bonding to the copper atoms sitting on three-fold hollow-sites, yet pulled away in the vertical direction, and the benzene ring interacting with the Au(1 1 1) substrate.

Analogously to the $[1\bar{1}0]$ direction, the chain geometry along the $[11\bar{2}]$ direction presents slightly tilted BTA species, their angle with the surface being ~15°. The molecular species present a further rotation around the C_2 axis (see Scheme 1b) with respect to the configuration along the $[1\bar{1}0]$ direction, so that the molecular plane is not parallel to the surface but inclined by ca. 30°. This extra rotation is due to the shorter distance of 5.1 Å (L^1 in Fig. 5b) between neighbouring copper adatoms in the $[11\bar{2}]$ direction with respect to the $[1\bar{1}0]$ direction. Opposite BTA species are 8.8 Å apart (L^2 in Fig. 5b). Also for this direction, the calculated distances are slightly shorter than the measured ones (see Fig. 4c, profile *C*). The longer distances could be related to the thermal drift seen in the STM images, which are collected at room temperature, whereas the DFT assumes 0 K.

Comparison of simulated STM images (central panels in Fig. 5) with the experimental STM images of Fig. 4 shows that both sets of chains produce a pattern which is compatible with the experimental system. In the "flatter" case of the chain along the $[1\bar{1}0]$ direction, some of the copper adatoms are visible in the calculated image, as seen in Fig. 5a. In the case of the more tilted molecular species chains orientated along the $[11\bar{2}]$ direction, only the carbon rings are visible instead. Moreover, in both cases, the electron densities make the molecular species appearing at an angle with respect to the direction of propagation of the chain, in agreement with the experimental observations (Fig. 4b).

On the rightmost column of Fig. 5 the simulated XP N 1s core level spectra of both systems are shown. Both calculated spectra reproduce well those collected after annealing to 393 K – 493 K (N 1s Fig. 2 panels c) and d). Excess molecules could generate the additional higher binding energy peak seen after preparation (N 1s Fig. 2 panel b) and in [30–31,66]. Considering that all Cu-N bonds are chemically equivalent, the difference in spectral fingerprint may originate from the different orientation of the -$[CuBTA]_n$- chains with respect to the Au(1 1 1) surface, and the varying tilt angle of each BTA species.

Regarding the energetics of the systems, before the deposition of copper atoms, the initial experimentally observed adsorbed structure is a series of hydrogen bonded BTAH chains, already investigated in [65]. Details of the structure are in SI9. Simulations of such chains on Au (1 1 1) show that the molecules physisorb on the surface with a free energy of adsorption per surface area (Eq. (3)) $E_1 = -18.25$ meV/Å^2. When the organometallic chains form, the stability of the system is promoted by the chemisorption of the azole moiety to the copper adatoms, and by the transition to a more compact structure which occupies a surface area which is roughly half with respect to that of the hydrogen bonded chains. The free energy of adsorption per surface area of these systems given in Eq. (4) is $E_2 = -60.45$ meV/Å^2 for the system in Fig. 5a and $E_2 = -63.53$ meV/Å^2 for the system in Fig. 5b, the negative number indicating that the transition between the hydrogen bonded chains and the organometallic ones is thermodynamically favoured.

It is worth noting that when the adsorption energy of BTA per unit molecule is considered to understand purely the strength of adsorption of the molecular species to the surface, using Eq. (5), it is found that the system in Fig. 5a is more stable than that in Fig. 5b, the adsorption energies being $E_{ads} = -4.22$ eV/mol and $E_{ads} = -4.16$ eV/mol respectively. Thus, the system of Fig. 5a, along the $[1\bar{1}0]$ direction, binds slightly more strongly to the surface, but occupies a larger surface area, than the system in Fig. 5b, along the $[11\bar{2}]$ direction. Regardless of that, the adsorption energies difference between the two systems is small, around 60 meV. This energy difference does not account for any kinetic effects which might affect the distribution of BTA species and copper atoms on the surface. The importance of kinetic effects is highlighted by the difference in the resulting systems when the copper atoms are deposited before [31] or after benzotriazole, as in this work. Thus, there is a high likelihood that the reaction of copper adatoms with benzotriazole results in structures propagating in several directions, as the STM image in Fig. 4a shows. When considering the hydrogen bonded BTAH chains, before addition of the copper adatoms, BTAH molecules physisorb on the surface with an adsorption energy $E_{ads} = -1.33$ eV/mol (SI7).,

These theoretical calculations definitely support the formation of -$[CuBTA]_n$- chains over other systems on the Au(1 1 1) surface.

3.3. Discussion

In a UHV environment BTAH has been reported to chemisorb dissociatively on pristine copper low index surfaces and to form ordered adlayers based on a generic $Cu_x(BTA)_y$ stoichiometry which include upright CuBTA [26–28], $Cu(BTA)_2$ [26–27] and chain structures [37], all anchored to the copper surfaces via copper adatoms. Additionally, combinations of the above [27,30–31] and flat-lying species have been reported [30–32]. Theoretical works have proposed adsorption models spanning from isolated molecules, oligomers, to polymerised species in various orientations, many involving the presence of adatoms [35–36,38–39]. To date the necklace polymer, predicted to be the most favourable on the (1 1 1) surface [36], has not been observed experimentally with certainty.

$Cu(BTA)_2$ species, requiring fewer adatoms than the -$[CuBTA]_n$- chains, are observed more often experimentally [26–28,66]. This suggests that the morphology of the low index surfaces might not have an adequate availability of adatoms by, e.g., not exposing enough defective sites, to produce the necklace polymer. On the one hand this indicates the necessity to work on more realistic substrates [76–77,81–83], and to investigate further the role of copper adatoms.

A strategy to highlight the role of copper adatoms is the use of an inert substrate over which both BTAH and copper are dosed, such as Au (1 1 1) surfaces. Herein copper atoms are added over an Au(1 1 1) surface pre-saturated with BTAH, thus arguably making them even more active than in ref [18–19,31]. In fact, upon dosing copper on Au(1 1 1), copper atoms incorporate into Au(1 1 1) [18–20,31,43–45], then react with BTAH and are segregated to the surface [20,31]. Related systems considering the behaviour of Cu/Au(1 1 1) [20,44–45,60], the adsorption of BTAH on copper single crystals [26–30,66], on Au(1 1 1) [65], and on Cu/Au(1 1 1) [31], to which comparison will be made, have been investigated separately elsewhere.

HREELS measurements show a spectrum dominated by signals generated by flat adsorbed hydrogen-bonded chains upon dosing BTAH (Fig. 1a). On addition of copper and upon annealing, the dominant species, essentially still flat-lying, is characterised by Cu-N bonds (Fig. 1c-d). Overall, the behaviour with increasing temperature is in agreement with the combined evidence derived initially from adsorption on Au(1 1 1) [65], and then on Cu/Au(1 1 1) [31].

Photoelectron spectroscopy measurements (Fig. 2) show that after annealing the hydrogen-bonded species desorb readily, whereas the organometallic species remain stable up to ca. 500 K. The Cu $2p_{3/2}$ peak stays essentially constant in BE, and its decrease can be correlated to the decrease of both N 1s and C 1s signals (Table 2). This points to desorption of a $Cu_x(BTA)_y$ compound, as was also the case for Cu(1 1 1) [27], Cu/Au(1 1 1) [31] and Ni(1 1 1) [80]. However, diffusion of copper atoms into the bulk cannot be ruled out.

In agreement with HREELS data, NEXAFS measurements (Fig. 3) confirm that, in contrast to flat-lying adsorption on Au(1 1 1) [65], and upright/mixed orientation on Cu(1 1 1) [26–28,30–31,37,66] and Cu/Au(1 1 1) [31], in the present work the adsorbed BTA moieties are flat-lying, yet not fully parallel to the surface. The adsorbed species after copper is added has some hydrogen-bonding character before annealing, as evidenced by the fine structure of the π^* transition, similar to that recorded on Au(1 1 1) [65]. Upon annealing a change in the fine structure of the π^* transition is recorded. This is ascribed to the formation of N-Cu bonds [28,30–31] and rendered evident by annealing, causing the preferential desorption of the hydrogen-bonded species. The overall orientation of the BTA moieties with respect to the surface does not appear to change much with increasing temperatures.

The STM contrast (Fig. 4) indicates that after addition of copper and mild annealing, the majority of adsorbates are flat chain-like species. In Fig. 4a, chains seem to propagate mainly along $\langle 1\bar{1}0\rangle$ and $\langle 11\bar{2}\rangle$ – types of directions and their concentration varying locally. From the images it cannot be unambiguously determined whether copper adatoms are incorporated into the adsorbed species. Some features at herringbone elbows can be ascribed to copper clusters decorated by benzotriazole, similarly to what seen on Cu/Au(1 1 1) [31 and figure S7b]. The flat-lying species are different from those observed on Au(1 1 1) [65 and Figures S5, and S9]. In the case of Au(1 1 1), a balance of intermolecular interactions (hydrogen-bonding and dispersive) and interaction with the substrate results in BTAH molecular chains with irregular periodicity (0.5 – 0.78 nm) and widths (0.63 – 0.73 nm) [65]. The different structures observed in this work are a clear indication of the effects of the added copper atoms. It is worth noting that for a similar coverage in copper, on Cu/Au(1 1 1) a few large copper related islands had formed [31], whereas in the present case a lot of small clusters at herring bone elbows can be seen. This is an indication that benzotriazole facilitates the dispersion of copper, as a consequence of copper atoms encountering BTAH and reacting with it, before landing on the Au(1 1 1) surface, making clear that the preparation recipe has important consequences on the resulting morphology.

DFT calculations show that copper adatoms allow BTAH to chemisorb on the Au(1 1 1) surface; moreover, the position of the copper adatoms on the surface determines whether BTA species adsorb flat or tilted. The average tilt angle has been found in agreement with that obtained via NEXAFS. On Cu(1 1 1) the central nitrogen atom in the triazole moiety, N_2, binds with a surface copper atom on one molecule, whereas does not on the adjacent molecule [37]. In that case, the copper adatom forced the molecular species to adopt an upright geometry. Instead, in the structures described in this work (Fig. 5), -[CuBTA]$_n$- chains are more closely packed, and all nitrogen atoms can bind with copper adatoms, not with copper surface atoms, resulting in chains with a flat structure. It is also worth noting that copper adatoms will stay almost in registry with the most energetically stable hollow sites, even though they are pulled away in the vertical direction by the interaction with BTA species. This indicates that the Cu - BTA interaction is slightly stronger than the Cu - Au one. This is seen clearly in the reversed system, where BTAH can segregate copper atoms form subsurface to the surface layer [31].

Even though copper adatoms are not sitting precisely in the hollow sites, the distance between neighbouring hollow sites on the surface seems to influence the structure of the chain, and in particular the spacing between adjacent BTA species, which induces tilts of the BTAs' molecular planes with respect to the surface. Such tilting is also the reason why BTA moieties appear orientated at an angle with respect to the direction of propagation of the chains, on STM images, as appears clear when comparison between the contrast observed in Fig. 4b and the calculated electron densities in Fig. 5 central panels is made. STM shows that chains run preferentially along high symmetry directions, indicating that the formation of Cu – BTA bonds and ultimately the condensation into the -[CuBTA]$_n$- chains is energetically of a similar order of magnitude than the interaction with the support.

Table 3 summarizes chain dimensions for the different systems considered. In the gas phase the change from hydrogen bonded to organometallic chains makes both L^1 and L^2 distances to contract, L^1 by far indicating the effect of the copper atoms. When hydrogen bonded chains are adsorbed on Au(1 1 1), the substrate has a minimal effect. However, for organometallic chains on Au(1 1 1) L^1 slightly expands and L^2 slightly contracts. This clearly shows the effect of the copper adatoms on the morphology of the chains. Simulations of hydrogen bonded and organometallic chains are reported in SI8.

Remarkably, this work shows evidence of the formation of -[CuBTA]$_n$- chains which, although theoretically predicted to be the most stable structures on Cu(1 1 1) [35,37], have not been experimentally observed so far [21–31,66]. When depositing BTAH on the Cu(1 1 1) surface, the copper adatoms necessary to stabilize the organometallic complexes have a costly formation energy of 0.8 eV per adatom [37], and, as a consequence, $Cu(BTA)_2$ species, which require fewer adatoms, form. On the other hand, here copper atoms are added to the system, and the adatoms' formation energy is no longer relevant, thus favouring the formation of the more stable chains shown in Fig. 5. One crucial difference is that the BTA moieties of the organometallic -[CuBTA]$_n$- chains on Cu(1 1 1), predicted via computational methods, are supposed to be orientated upright, whereas those prepared in this work are lying flat.

4. Conclusion

In this work, the role of copper atoms in the room temperature adsorption of BTAH on Au(1 1 1) has been investigated using

Table 3
Summary of L^1 and L^2 (defined as in Fig. 5) distances in Å for the systems considered.

system	DFT		STM	
	L^1	L^2	L^1	L^2
Gas phase -[BTAH]$_n$-	9.37	9.64	–	–
Gas phase -[CuBTA]$_n$-	4.90	9.22	–	–
-[BTAH]$_n$-/Au(1 1 1)	10.16	7.75	6.8 [65]	6.3–7.3 [65]
-[CuBTA]$_n$-/Au(1 1 1); $[1\bar{1}0]$	5.9	8.7	6.6	8.2
-[CuBTA]$_n$-/Au(1 1 1); $[11\bar{2}]$	5.1	8.8	5.8	7.6

complementary surface sensitive techniques and theoretical calculations.

A way to enhance the reactivity of copper is to dose it from the gas phase onto BTAH precovered Au(1 1 1) surfaces, in an attempt to highlight the role reactive atoms can play when reaching the surface.

The techniques that give direct access to orientational information (HREELS, NEXAFS) indicate that the structures that have been prepared are flat lying overall. The presence of both hydrogen-bonded and organometallic structures and the persistence of the organometallic structures after mild annealing is determined from XPS, NEXAFS, and HREELS. STM shows that organometallic structures can propagate in several directions and have homogeneous contrast overall. DFT modelling shows that the prepared structures are essentially chemically equivalent and almost degenerate.

Rationalisation of the role of the copper adatoms comes from the comparison between experimental measurements and DFT modelling. The adsorption site of copper adatoms and the relative mobility of the adlayer are crucial factors in determining the resulting Cu-BTA organometallic structure; favourable copper adatoms adsorption sites on the Au(1 1 1) surface are almost maintained and presumably strengthen by van der Waals interactions between the aromatic systems and the metal surface.

This hints to the possibility of creating chain structures of BTAH on copper surfaces by adding metal atoms post-organic deposition, and more generally, of engineering organometallic structures on surfaces exploting the relevant adatoms.

CRediT authorship contribution statement

Federico Grillo: Conceptualization, Data curation, Formal analysis, Funding acquisition, Investigation, Project administration, Visualization, Writing – original draft, Writing – review & editing. **Chiara Gattinoni:** Data curation, Formal analysis, Investigation, Visualization, Writing – review & editing. **Christian R. Larrea:** Investigation. **Paolo Lacovig:** Investigation, Writing – review & editing. **Neville V. Richardson:** Conceptualization, Funding acquisition, Writing – review & editing.

Declaration of Competing Interest

The authors declare that they have no known competing financial interests or personal relationships that could have appeared to influence the work reported in this paper.

Acknowledgements

FG has received funding from the European Community's Seventh Framework Programme (FP7/2007-2013) under grant agreement n° 312284 for part of the research leading to these results (NEXAFS, XPS). The Engineering and Physical Sciences Research Council (EPSRC) is acknowledged for the funding of CRL's PhD studentship – EP/M506631/1. Prof. Christopher J. Baddeley (University of St. Andrews) and Dr. Silvano Lizzit (SuperESCA beam line, Elettra) are thanked for fruitful discussions. CG acknowledges the Euler cluster managed by the HPC team at ETH Zurich for computational resources. FG acknowledges the EaStCHEM Research Computing facility for providing computational resources for the gas phase modelling of HREELS data.

The research data supporting this publication can be accessed at https://doi.org/10.17630/19a5e783-c2ea-4f24-993c-d037cd602145

Appendix A. Supplementary data

Derivation of Gibbs adsorption energies, gas phase modelling, XPS binding energies comparison, average angle of triazole ring from NEXAFS, additional STM images, summary of trial structures optimised via DFT, simulation of H-bonded BTAH chains on Au(1 1 1), H-bonded and organometallic gas phase chains. Supplementary data to this article can be found online at https://doi.org/10.1016/j.apsusc.2022.154087.

References

[1] A. Chaudhuri, T.J. Lerotholi, D.C. Jackson, D.P. Woodruff, V.R. Dhanak, The local adsorption structure of methylthiolate and butylthiolate on Au(1 1 1): A photoemission core-level shift investigation, Surf. Sci. 604 (2010) 227–234.
[2] P. Maksymovych, O. Voznyy, D.B. Dougherty, D.C. Sorescu, J.T. Yates, Gold adatom as a key structural component in self-assembled monolayers of organosulfur molecules on Au(1 1 1), Prog. Surf. Sci. 85 (2010) 206–240.
[3] B.G. Frederick, F.M. Leibsle, S. Haq, N.V. Richardson, Evolution of Lateral order and molecular reorientation in the benzoate/Cu(110) system, Surf. Rev. Lett. 4 (1996) 1523–1546.
[4] Q. Chen, C.C. Perry, B.G. Frederick, P.W. Murray, S. Haq, N.V. Richardson, Structural aspects of the low-temperature deprotonation of benzoic acid on Cu (110) surfaces, Surf. Sci. 446 (2000) 63–75.
[5] C.C. Perry, S. Haq, B.G. Frederick, N.V. Richardson, Face specificity and the role of metal adatoms in molecular reorientation at surfaces, Surf. Sci. 409 (1998) 512–520.
[6] M.N. Faraggi, C. Rogero, A. Arnau, M. Trelka, D. Écija, C. Isvoranu, J. Schnadt, C. Marti-Gastaldo, E. Coronado, J.M. Gallego, R. Otero, R. Miranda, Role of Deprotonation and Cu Adatom Migration in Determining the Reaction Pathways of Oxalic Acid Adsorption on Cu(111), J. Phys. Chem. C 115 (2011) 21177–21182.
[7] M.C. Lennartz, N. Atodiresei, L. Müller-Meskamp, S. Karthäuser, R. Waser, S. Blügel, Cu-Adatom-Mediated Bonding in Close-Packed Benzoate/Cu(110)-Systems, Langmuir 25 (2009) 856–864.
[8] S. Poulston, A. Jones, R.A. Bennett, M. Bowker, An STM investigation of formic acid adsorption on oxygen precovered Cu(110), Surf. Sci. 377–379 (1997) 66–70.
[9] S. Jensen, C.J. Baddeley, Formation of PTCDI-Based Metal Organic Structures on a Au(111) Surface Modified by 2-D Ni Clusters, J. Phys. Chem. C 112 (2008) 15439–15448.
[10] A.E. Anderson, F. Grillo, C.R. Larrea, R.T. Seljamäe-Green, H.A. Früchtl, C. J. Baddeley, Metallosupramolecular Assembly of Cr and p-Terphenyldinitrile by Dissociation of Metal Carbonyls on Au(111), J. Phys. Chem. C 120 (2016) 1049–1055.
[11] A.C. Papageorgiou, J. Li, S.C. Oh, B. Zhang, Ö. Sağlam, Y. Guo, J. Reichert, A. B. Marco, D. Cortizo-Lacalle, A. Mateo-Alonso, J.V. Barth, Tuning the ease of formation of on-surface metal-adatom coordination polymers featuring diketones, Nanoscale 10 (2018) 9561–9568.
[12] P. Knecht, N. Suryadevara, B. Zhang, J. Reichert, M. Ruben, J.V. Barth, S. Klyatskaya, A.C. Papageorgiou, The self-assembly and metal adatom coordination of a linear bis-tetrazole ligand on Ag(111), Chem. Commun. 54 (2018) 10072–10075.
[13] F. Grillo, H. Früchtl, S.M. Francis, V. Mugnaini, M. Oliveros, J. Veciana, N. V. Richardson, An ordered organic radical adsorbed on a Cu-doped Au(111) surface, Nanoscale 4 (2012) 6718–6721.
[14] J. Liu, T. Lin, Z. Shi, F. Xia, L. Dong, P.N. Liu, N. Lin, Structural Transformation of Two-Dimensional Metal-Organic Coordination Networks Driven by Intrinsic In-Plane Compression, J. Am. Chem. Soc. 133 (2011) 18760–18766.
[15] Z. Shi, N. Lin, Structural and Chemical Control in Assembly of Multicomponent Metal−Organic Coordination Networks on a Surface, J. Am. Chem. Soc. 132 (2010) 10756–10761.
[16] S.L. Tait, Y. Wang, G. Costantini, N. Lin, A. Baraldi, F. Esch, L. Petaccia, S. Lizzit, K. Kern, Metal−Organic Coordination Interactions in Fe−Terephthalic Acid Networks on Cu(100), J. Am. Chem. Soc. 130 (2008) 2108–2113.
[17] A. Dmitriev, H. Spillmann, N. Lin, J.V. Barth, K. Kern, Modular Assembly of Two-Dimensional Metal-Organic Coordination Networks at a Metal Surface, Angew. Chem. Int. Ed. 42 (2003) 2670–2673.
[18] L. Wang, P. Li, H. Shi, Z. Li, K. Wu, X. Shao, Thickness-Dependent Adsorption of Melamine on Cu/Au(111) Films, J. Phys. Chem. C 121 (2017) 7977–7984.
[19] H. Shi, W. Wang, Z. Li, L. Wang, X. Shao, Tailoring the Self-assembly of Melamine on Au(111) via Doping with Cu Atoms, Chin. J. Chem. Phys. 30 (2017) 443–449.
[20] F. Grillo, R. Megginson, J. Christie, S.M. Francis, N.V. Richardson, C.J. Baddeley, Structure and Reactivity of Cu-doped Au(111) Surfaces, e-J, Surf. Sci. Nanotec. 16 (2017) 163–171.
[21] L. Jiang, B. Zhang, A.P. Seitsonen, F. Haag, F. Allegretti, J. Reichert, B. Kuster, J. V. Barth, A.C. Papageorgiou, N-Heterocyclic carbenes on close-packed coinage metal surfaces: bis-carbene metal adatom bonding scheme of monolayer films on Au, Ag and Cu, Chem. Sci. 8 (2017) 8301–8308.
[22] E. Angove, F. Grillo, H.A. Früchtl, A.J. Veinot, I. Singh, J.H. Horton, C.M. Crudden, C.J. Baddeley, Highly ordered N-heterocyclic carbene monolayers on Cu (111), J. Phys. Chem. Lett. 13 (2022) 2051–2056.
[23] M.M. Antonijević, M.B. Petrović, Copper Corrosion Inhibitors. A review, Int. J. Electrochem. Sci. 3 (2008) 1–28.
[24] M. Finšgar, I. Milošev, Inhibition of copper corrosion by 1,2,3-benzotriazole: A review, Corros. Sci. 52 (2010) 2737–2749.
[25] M.B.Petrović Mihajlović, M.M. Antonijević, Copper corrosion inhibitors. Period 2008-2014, a review, Int. J. Electrochem. Sci. 10 (2015) 1027–1053.
[26] F. Grillo, D.W. Tee, S.M. Francis, H. Früchtl, N.V. Richardson, Initial stages of benzotriazole adsorption on the Cu(111) surface, Nanoscale 5 (2013) 5269–5273.
[27] F. Grillo, D.W. Tee, S.M. Francis, H.A. Früchtl, N.V. Richardson, Passivation of Copper: Benzotriazole Films on Cu(111), J. Phys. Chem. C 118 (2014) 8667–8675.
[28] J.F. Walsh, H.S. Dhariwal, A. Gutierrez-Sosa, P. Finetti, C.A. Muryn, N.B. Brookes, R.J. Oldman, J. Thornton, Probing molecular orientation in corrosion inhibition

via a NEXAFS study of benzotriazole and related molecules on Cu(100), Surf. Sci. 415 (1998) 423–432.
[29] B.S. Fang, C.G. Olson, D.W. Lynch, A photoemission study of benzotriazole on clean copper and cuprous oxide, Surf. Sci. 176 (1986) 476–490.
[30] C. Gattinoni, P. Tsaousis, C. Euaruksakul, R. Price, D.A. Duncan, T. Pascal, D. Prendergast, G. Held, A. Michaelides, Adsorption Behavior of Organic Molecules: A Study of Benzotriazole on Cu(111) with Spectroscopic and Theoretical Methods, Langmuir 35 (2019) 882–893.
[31] F. Grillo, D. Batchelor, C.R. Larrea, S.M. Francis, P. Lacovig, N.V. Richardson, On-surface condensation of low-dimensional benzotriazole–copper assemblies, Nanoscale 11 (2019) 13017–13031.
[32] R.F. Roberts, X-ray photoelectron spectroscopic characterization of copper oxide surfaces treated with benzotriazole, J. Electron. Spectrosc. Relat. Phenom. 4 (1974) 273–291.
[33] J.C. Rubim, I.G.R. Gutz, O. Sala, W.J. Orville-Thomas, Surface enhanced Raman spectra of benzotriazole adsorbed on a copper electrode, J. Mol. Struct. 100 (1983) 571–583.
[34] Y. Jiang, J.B. Adams, First principle calculations of benzotriazole adsorption onto clean Cu(1 1 1), Surf. Sci. 529 (2003) 428–442.
[35] A. Kokalj, *Ab initio* modeling of the bonding of benzotriazole corrosion inhibitor to reduced and oxidized copper surfaces, Faraday Discuss. 180 (2015) 415–438.
[36] X. Chen, H. Hakkinen, Divide and Protect: Passivating Cu(111) by Cu-(benzotriazole)$_2$, J. Phys. Chem. C 116 (2012) 22346–22349.
[37] C. Gattinoni, A. Michaelides, Understanding corrosion inhibition with van der Waals DFT methods: the case of benzotriazole, Faraday Discuss. 180 (2015) 439–458.
[38] A. Kokalj, S. Peljhan, M. Finšgar, I. Milošev, What Determines the Inhibition Effectiveness of ATA, BTAH, and BTAOH Corrosion Inhibitors on Copper? J. Am. Chem. Soc. 132 (2010) 16657–16668.
[39] D. Gopi, K.M. Govindaraju, V. Collins Arun Prakash, D.M. Angeline Sakila, L. Kavitha, A study on new benzotriazole derivatives as inhibitors on copper corrosion in ground water, Corros. Sci. 51 (2009) 2259–2265.
[40] Y. Gong, Z. Wang, F. Gao, S. Zhang, H. Li, Synthesis of New Benzotriazole Derivatives Containing Carbon Chains as the Corrosion Inhibitors for Copper in Sodium Chloride Solution, Ind. Eng. Chem. Res. 54 (2015) 12242–12253.
[41] C.R. Larrea, C.J. Baddeley, M.R. Narouz, N.J. Mosey, J.H. Horton, C.M. Crudden, *N*-Heterocyclic Carbene Self-assembled Monolayers on Copper and Gold: Dramatic Effect of Wingtip Groups on Binding, Orientation and Assembly, ChemPhysChem 18 (2017) 3536–3539.
[42] C.M. Crudden, J.H. Horton, I.I. Ebralidze, O.V. Zenkina, A.B. McLean, B. Drevniok, Z. She, H.-B. Kraatz, N.J. Mosey, T. Seki, E.C. Keske, J.D. Leake, A. Rousina-Webb, G. Wu, Ultra stable self-assembled monolayers of N-heterocyclic carbenes on gold, Nat. Chem. 6 (2014) 409–414.
[43] F. Grillo, H. Früchtl, S.M. Francis, N.V. Richardson, Site selectivity in the growth of copper islands on Au (111), New J. Phys. 13 (2011) 013044.
[44] F. Grillo, R. Megginson, D. Batchelor, M. Muntwiler, C.J. Baddeley, Structural and electronic characterisation of Cu/Au(111) near-surface alloys, Jpn. J. Appl. Phys. 58 (2019) SIIB09.
[45] M. Kuhn, T.K. Sham, Charge redistribution and electronic behavior in a series of Au-Cu alloys, Phys. Rev. B 49 (1994) 1647–1661.
[46] A. Baraldi, M. Barnaba, B. Brena, D. Cocco, G. Comelli, S. Lizzit, G. Paolucci, R. Rosei, Time resolved core level photoemission experiments with synchrotron radiation, J. Electron. Spectrosc. Relat. Phenom. 76 (1995) 145–149.
[47] A. Baraldi, G. Comelli, S. Lizzit, M. Kiskinova, G. Paolucci, Real-time X-ray photoelectron spectroscopy of surface reactions, Surf. Sci. Rep. 49 (2003) 169–224.
[48] G. Cautero, R. Sergo, L. Stebel, P. Lacovig, P. Pittana, M. Predonzani, S. Carrato, A two-dimensional detector for pump-and-probe and time resolved experiments, Nucl. Instrum. Meth. A 595 (2008) 447–459.
[49] J. Stöhr, NEXAFS spectroscopy, in: R. Gomer (Ed.), Springer Series in Surface Science, vol. 25, Springer, Berlin, 1992.
[50] B. Ravel, M. Newville, ATHENA, ARTEMIS, HEPHAESTUS: data analysis for X-ray absorption spectroscopy using IFEFFIT, J. Synchrotron Radiat. 12 (2005) 537–541.
[51] J. Stöhr, D.A. Outka, Determination of molecular orientations on surfaces from the angular dependence of near-edge x-ray-absorption fine-structure spectra, Phys. Rev. B: Condens. Matter Mater. Phys. 36 (1987) 7891–7905.
[52] CasaXPS software version 2.3.17 (Casa Software Ltd, Teignmouth, UK).
[53] J.J. Yeh, Atomic Calculation of Photoionization Cross-Sections and Asymmetry Parameters, Gordon and Breach Science Publishers, Langhorne, PE (USA), 1993.
[54] J.J. Yeh, I. Lindau, Atomic subshell photoionization cross sections and asymmetry parameters: $1 \leqslant Z \leqslant 103$, At. Data Nucl. Data Tables 32 (1985) 1–155.
[55] I. Horcas, R. Fernández, J.M. Gómez-Rodríguez, J. Colchero, J. Gómez-Herrero, A. M. Baro, WSXM: A software for scanning probe microscopy and a tool for nanotechnology, Rev. Sci. Instrum. 78 (2007) 013705.
[56] G. Kresse, J. Hafner, *Ab initio* molecular dynamics for liquid metals, Phys. Rev. B 47 (1993) 558–561.
[57] G. Kresse, J. Hafner, *Ab initio* molecular-dynamics simulation of the liquid-metal–amorphous-semiconductor transition in germanium, Phys. Rev. B 49 (1994) 14251–14269.
[58] J. Klimeš, D.R. Bowler, A. Michaelides, Chemical accuracy for the van der Waals density functional, J. Phys.: Cond. Matt. 22 (2010) 022201.
[59] G. Kresse, D. Joubert, From ultrasoft pseudopotentials to the projector augmented-wave method, Phys. Rev. B 59 (1999) 1758–1775.
[60] H. Aitchison, N. Meyerbröker, T.-L. Lee, J. Zegenhagen, T. Potter, H.A. Früchtl, I. Cebula, M. Buck, Underpotential deposition of Cu on Au(111) from neutral chloride containing electrolyte, PhysChemChemPhys 19 (2017) 24146–24153.
[61] K. Reuter, M. Scheffler, Composition, structure, and stability of RuO_2(110) as a function of oxygen pressure, Phys. Rev. B 65 (2002) 035406.
[62] A.T. Lozovoi, A. Alavi, M.W. Finnis, Surface energy and the early stages of oxidation of NiAl(110), Comp. Phys. Comm. 137 (2001) 174–194.
[63] L. Köhler, G. Kresse, Density functional study of CO on Rh(111), Phys. Rev. B 70 (2004) 165405.
[64] M.J. Frisch, G.W. Trucks, H.B. Schlegel, G.E. Scuseria, M.A. Robb, J.R. Cheeseman, G. Scalmani, G. Barone, B. Mennucci, G.A. Petersson, et al., Gaussian 09, Revision D.01, Gaussian Inc., Wallingford CT, 2013.
[65] F. Grillo, J.A. Garrido Torres, M.-J. Treanor, C.R. Larrea, J.P. Götze, P. Lacovig, H. A. Früchtl, R. Schaub, N.V. Richardson, Two-dimensional self-assembly of benzotriazole on an inert substrate, Nanoscale 8 (2016) 9167–9177.
[66] M. Turano, M. Walker, F. Grillo, C. Gattinoni, J. Edmondson, O. Adesida, G. Hunt, P. Kirkman, N.V. Richardson, C.J. Baddeley, A. Michaelides, G. Costantini, Understanding the interaction of organic corrosion inhibitors with copper at the molecular scale: Benzotriazole on Cu(110), Appl. Surf. Sci. 570 (2021) 151206.
[67] I. Popova, J.T. Yates Jr., Adsorption and Thermal Behavior of Benzotriazole Chemisorbed on γ-Al_2O_3, Langmuir 13 (1997) 6169–6175.
[68] L.F. Peña, J.-F. Veyan, M.A. Todd, A. Derecskei-Kovacs, Y.J. Chabal, Vapor-Phase Cleaning and Corrosion Inhibition of Copper Films by Ethanol and Heterocyclic Amines, ACS Appl. Mater. Interfaces 10 (2018) 38610–38620.
[69] K. Salorinne, X. Chen, R.W. Troff, M. Nissinen, H. Häkkinen, One-pot synthesis and characterization of subnanometre-size benzotriazolate protected copper clusters, Nanoscale 4 (2012) 4095–4098.
[70] C. Toernkvist, J. Bergman, B. Liedberg, Geometry and vibrations of the 1, 2, 3-triazole anion. A theoretical and experimental study, J. Phys. Chem. 95 (1991) 3119–3123.
[71] B. Gao, B. Tan, Y. Liu, C. Wang, Y. He, Y. Huang, A study of FTIR and XPS analysis of alkaline-based cleaning agent for removing Cu-BTA residue on Cu wafer, Surf. Interface Anal. 51 (2019) 566–575.
[72] X-ray Photoelectron Spectroscopy Database Version 4.1, National Institute of Standards and Technology, Gaithersburg (2012) (Accessed Jan 2022); http://srdata.nist.gov/xps/.
[73] D. Tahir, S. Tougaard, Electronic and optical properties of Cu, CuO and Cu_2O studied by electron spectroscopy, J. Phys. Condens. Matter 24 (2012) 175002.
[74] C.D. Wagner, W.M. Kiggs, L.E. Davis, J.F. Moulder, Handbook of X-ray Photoelectron Spectroscopy, Perkin-Elmer Corporation-Physical Electronics Division, Eden Prairie, MN, 1979.
[75] A. Kokalj, S. Peljhan, J. Koller, The Effect of Surface Geometry of Copper on Dehydrogenation of Benzotriazole. Part II, J. Phys. Chem. C 118 (2014) 944–954.
[76] M. Finšgar, J. Kovač, I. Milošev, Surface Analysis of 1-Hydroxybenzotriazole and Benzotriazole Adsorbed on Cu by X-Ray Photoelectron Spectroscopy, J. Electrochem. Soc. 157 (2010) C52–C60.
[77] A. Mirarco, S.M. Francis, C.J. Baddeley, A. Glisenti, F. Grillo, Effect of the pH in the growth of benzotriazole model layers at realistic environmental conditions, Corr. Sci. 143 (2018) 107–115.
[78] S. Poulston, P.M. Parlett, P. Stone, M. Bowker, Surface Oxidation and Reduction of CuO and Cu2O Studied Using XPS and XAES, Surf. Interface Anal. 24 (1996) 811–820.
[79] A. Mezzi, E. Angelini, T. De Caro, S. Grassini, F. Faraldi, C. Riccucci, G.M. Ingo, Investigation of the benzotriazole inhibition mechanism of bronze disease, Surf. Interface Anal.: ECASIA 44 (2012) 968–971.
[80] C.C. Chusuei, J.V. de la Peña, J.A. Schreifels, Contour temperature programmed desorption for monitoring multiple chemical reaction products, Rev. Sci. Instrum. 70 (1999) 3719–3722.
[81] A. Fateh, M. Aliofkhazraei, A.R. Rezvanian, Review of corrosive environments for copper and its corrosion inhibitors, Arabian, J. Chem. 13 (2020) 481–544.
[82] P.F. Khan, V. Shanthi, R.K. Babu, S. Muralidharan, R.C. Barik, Effect of benzotriazole on corrosion inhibition of copper under flow conditions, J. Environ. Chem. Eng. 3 (2015) 10–19.
[83] Y.-H. Lee, M.-S. Hong, S.-J. Ko, J.-G. Kim, Effect of Benzotriazole on the Localized Corrosion of Copper Covered with Carbonaceous Residue, Materials 14 (2021) 2722.